Evaluating the influence of the deformation of the forming tools in the thickness distribution along the wall of a cylindrical cup

To cite this article: M C Oliveira *et al* 2022 *IOP Conf. Ser.: Mater. Sci. Eng.* **1238** 012079

Evaluating the influence of the deformation of the forming tools in the thickness distribution along the wall of a cylindrical cup

M C Oliveira[1,*], D M Neto[1], A.F.G. Pereira[1], J L Alves[2] and LF Menezes[1]

[1]CEMMPRE, Department of Mechanical Engineering, University of Coimbra, Polo II, Rua Luís Reis Santos, Pinhal de Marrocos, 3030-788 Coimbra, Portugal
[2]CMEMS, Microelectromechanical Systems Research Unit, University of Minho, Campus de Azurém, Guimarães, 4800-058, Portugal

[*]E-mail: marta.oliveira@dem.uc.pt

Abstract. The Swift cup drawing test has been adopted for evaluating sheet metal deformation properties, namely the material formability assessed through the limiting drawing ratio. Since the strain path of the points located on the flange is between uniaxial compression and pure shear, this region is subjected to thickening. If the thickness of the drawn flange is larger than the gap between the punch and the die, cup wall ironing will occur. Therefore, the ironing forces can lead to significant elastic deformation of the forming tools (punch and die). The main objective of this study is to evaluate numerically the deformation of the forming tools during the deep drawing-ironing process of a cylindrical cup. Then, the effect of that deformation on both the earing profile and the evolution of thickness along the circumferential direction, at different heights, is analysed. The material studied is the AA 6016-T4. Since both the thickness strain and the earing profile are strongly influenced by the adopted yield criterion, the study considers the classical quadratic one proposed by Hill and a non-quadratic proposed by Cazacu and Barlat. The process conditions considered are the ones from EXACT, the ESAFORM Benchmark 2021, enabling the comparison with experimental results.

1. Introduction

The tools used in sheet metal forming processes are commonly made from carbon and alloy steels with distinct characteristics, such as hardness, wear resistance, toughness, and resistance to softening at elevated temperatures. Besides, comparing the geometry of the forming tools with the blank, the tools are significatively stiffer. This enables adopting the assumption that they can be treated like rigid bodies, in the numerical simulation of sheet metal forming processes. This simplifies the contact algorithms reducing the computational effort. Nevertheless, in some cases this assumption can lead to inaccurate predictions of the material flow and, consequently, of the thickness distribution [1]. The elastic deformation of the tools depends on their geometry, mechanical properties and magnitude of the contact forces. Therefore, the accurate prediction of the tools deformation requires their modelling and treatment as a solid deformable body, leading to a considerable increase of the computational time.

This study presents the finite element analysis of the deep drawing of a cylindrical cup, considering that the forming tools are modelled either as rigid or as deformable bodies. The numerical results are compared with the experimental ones, in order to assess the impact of the tools deformation resulting from the ironing stage.

2. Swift cup drawing test

The forming conditions adopted in this study correspond to the ones defined in the ESAFORM 2021 Benchmark: EXACT - Experiment and Analysis of Aluminum Cup Drawing Test [2]. The tools consist of a cylindrical punch with a flat bottom, a blank holder and a die, as schematically shown in Figure 1. The drawing operation is performed considering a constant blank holder force of 40 kN. Moreover, a stopper with the same thickness of the blank was used to avoid the pinching of the ears. The AA 6016-T4 blank sheet is circular in shape with a diameter of 107.5 mm and a thickness of 0.98 mm. The ESAFORM 2021 benchmark committee did not recommended a value for the friction coefficient. The results for the punch force evolution with its displacement and the earing profile were supplied to enable the participants the adjustment of its value. All details about the experimental procedure for the characterization of the material behaviour and forming of the cup are described in [3].

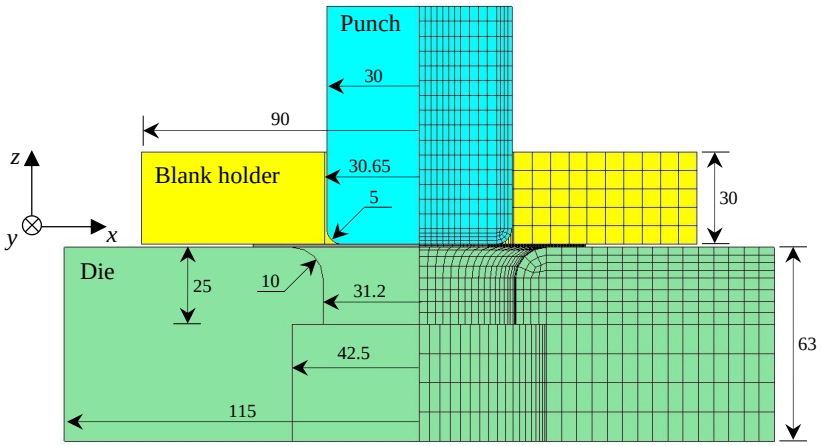

Figure 1. Schematic representation of the forming tools including main dimensions [mm] and the mesh adopted when considering deformable tools.

2.1. Mechanical behaviour

The mechanical behaviour of the AA 6016-T4 aluminium alloy is assumed to be isotropic in the elastic regime, being described by the Young's modulus, E, and the Poisson ratio, υ. Regarding the hardening behaviour, the Swift law suggested by the benchmark committee was adopted. The orthotropic behaviour was mainly described by the Hill'48 yield criterion, described by the equation

$$\bar{\sigma}^2 = F\left(\sigma_{22}-\sigma_{33}\right)^2 + G\left(\sigma_{33}-\sigma_{11}\right)^2 + H\left(\sigma_{11}-\sigma_{22}\right)^2 + 2L\tau_{23}^2 + 2M\tau_{13}^2 + 2N\tau_{12}^2 \quad (1)$$

where σ_{ij}, $i,j=1,2,3$ are the stress components of the Cauchy stress tensor $\boldsymbol{\sigma}$, defined in the principal axes of orthotropy, and F, G, H, L, M and N are the material parameters describing the anisotropy of the metal sheet. $\bar{\sigma}$ is the equivalent stress, which is equal to the flow stress, Y, under loading conditions. The parameters were determined based on the Lankford values for the rolling, diagonal and transverse directions and assuming that the flow stress corresponds to the stress-strain curve along the rolling direction ($G+H=1$). The L and M are the anisotropy parameters corresponding to the off-plane properties that cannot be evaluated for metallic sheets. Thus, they are assumed as equal to the isotropic values, i.e. 1.5.

Since an associated flow rule is adopted, in order to improve the understanding about the influence of the normal to the yield surface on the thickness distribution predicted, the yield criterion proposed by Cazacu and Barlat in 2001 (CB2001) [4] was also considered. The CB2001 is a generalization of the Drucker's isotropic criterion to orthotropy, such that:

$$\bar{\sigma} = \left\{27\left[\left(J_2^0\right)^3 - c\left(J_3^0\right)^2\right]\right\}^{\frac{1}{6}} \quad (2)$$

where J_2^0 and J_3^0 are the second and third generalized invariants of the deviatoric Cauchy stress tensor, defined as:

$$J_2^0 = \frac{a_1}{6}(\sigma_{11}-\sigma_{22})^2 + \frac{a_2}{6}(\sigma_{11}-\sigma_{33})^2 + \frac{a_3}{6}(\sigma_{11}-\sigma_{33})^2 + a_4\sigma_{12}^2 + a_5\sigma_{13}^2 + a_6\sigma_{23}^2 \tag{3}$$

$$\begin{aligned} J_3^0 = {} & (1/27)(b_1+b_2)\sigma_{11}^3 + (1/27)(b_3+b_4)\sigma_{22}^3 + (1/27)[2(b_1+b_4)-b_2-b_3]\sigma_{33}^3 \\ & -(1/9)(b_1\sigma_{22}+b_2\sigma_{33})\sigma_{11}^2 - (1/9)(b_3\sigma_{33}+b_4\sigma_{11})\sigma_{22}^2 \\ & -(1/9)[(b_1-b_2+b_4)\sigma_{11}+(b_1-b_3+b_4)\sigma_{22}]\sigma_{33}^2 \\ & +(2/9)(b_1+b_4)\sigma_{11}\sigma_{22}\sigma_{33} - (\sigma_{13}^2/3)[2b_9\sigma_{22}-b_8\sigma_{33}-(2b_9-b_8)\sigma_{11}] \\ & -(\sigma_{12}^2/3)[2b_{10}\sigma_{33}-b_5\sigma_{22}-(2b_{10}-b_5)\sigma_{11}] - (\sigma_{23}^2/3)[(b_6-b_7)\sigma_{11}-b_6\sigma_{22}-b_7\sigma_{33}] \\ & +2b_{11}\sigma_{12}\sigma_{23}\sigma_{13} \end{aligned} \tag{4}$$

where $a_1,...,a_6$ and $b_1,...,b_{11}$ are the anisotropy parameters and c is a weighting parameter. The conditions that guarantee the convexity of CB2001 are unknown, except when assuming in-plane isotropic behaviour, for which $c \in [-3.75, 2.25]$. In this case, the a_5, a_6 and b_k $(k = 6, 7, 8, 9, 11)$ are the anisotropy parameters corresponding to the off-plane properties, for which the isotropic values, i.e. 1.0 are assumed. The anisotropy parameters were identified considering the normalized tensile yield stresses and *r*-ratios extracted from uniaxial tensile tests performed at every 15º, between the rolling and the transverse directions, and the direction of the plastic strain-rate, extracted from biaxial tests performed with cruciform specimens. The material parameters adopted are all available in [3].

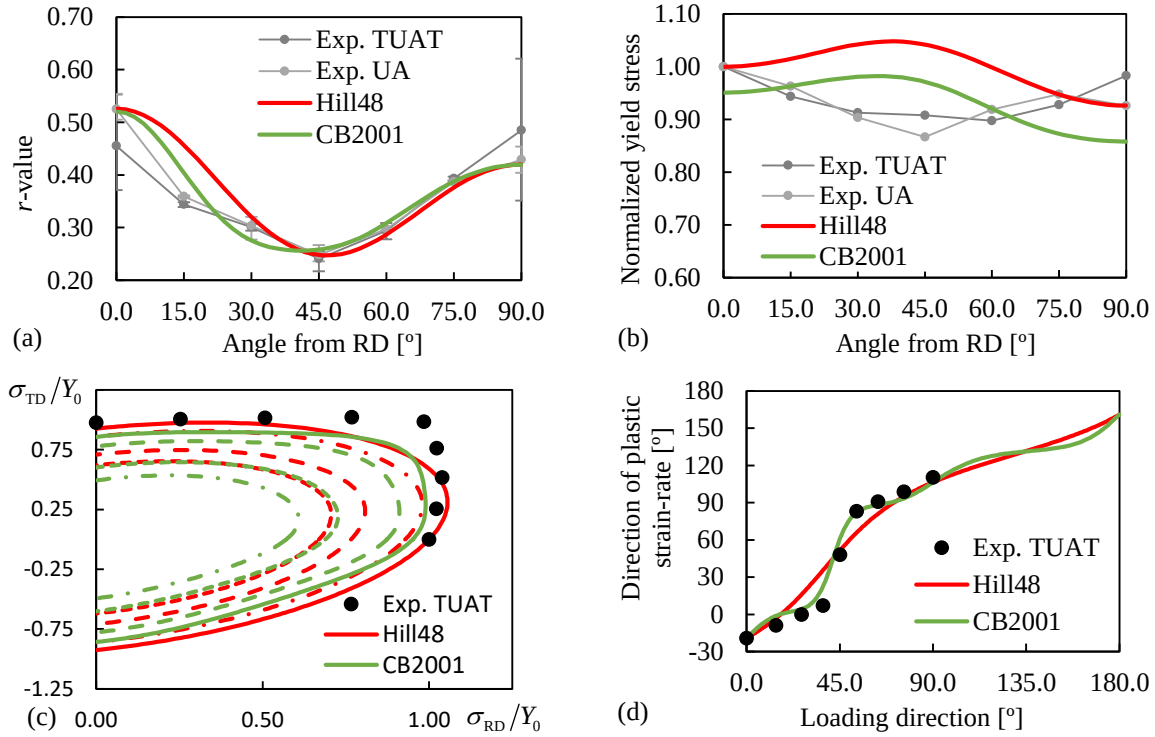

Figure 2. Comparison between experimental and predicted: (a) *r*-values; (b) yield stresses; (c) projection of the yield surface in the biaxial plane $(\sigma_{RD};\sigma_{TD})$ (with $\tau_{RD}/Y_0 = 0.0; 0.25; 0.43; 0.50$) and (d) direction of the plastic strain-rate. All stresses are normalized by the yield stress along the rolling direction Y_0.

Figure 2 presents the comparison between the experimental results (obtained by the Tokyo University of Agriculture and Technology (TUAT) and by the University of Aveiro (UA)) [3]. For both yield criteria, the uniaxial tensile test results considered in the identification were the ones obtained by UA. Figure 2 shows that both yield criteria lead to a similar in-plane evolution of the *r*-values and an identical trend for the normalized yield stress; both yield criteria describe well the experimental *r*-values but are unable to capture the yield stress distribution. Nevertheless, the projection of the yield surface in the biaxial plane shows that both yield surfaces present quite different descriptions of the shear stresses. Moreover, the direction of plastic strain-rate is also quite different for both yield criteria, as shown in Figure 2 (d), which highlights the flexibility of the CB2001.

2.2. Finite Element model: rigid tools

Due to geometrical and material symmetries, only a quarter of the global structure is modelled. In a first approach, all forming tools are considered rigid and are modelled using Nagata patches [5], which allows the use of a coarse finite element mesh. The contact with friction conditions are described by the Coulomb's law. As previously mentioned, there was no recommendation for a value for the friction coefficient. Therefore, a constant value for the friction coefficient was considered (μ=0.07) in order to best describe the drawing force.

The blank sheet is discretized with 3D 8-node hexahedral finite elements, combined with a selective reduced integration technique. The mesh comprises a non-structured mesh for a radius lower than 22 mm (bottom of the cup) and a structured mesh for the remaining region. The mesh is composed of two layers through the thickness, which allows an accurate evaluation of the contact forces and the through-thickness stress gradients. The total number of elements is 15408 and the total number of nodes is 16006.

2.2.1. Results analysis and discussion. Figure 3 (a) presents the punch force evolution with its displacement, comparing the experimental result with the one obtained with rigid tools. The results show that, although the constant value of μ=0.07 enables an accurate description of the drawing force, the ironing force is clearly overestimated. Moreover, the analysis of the thickness distribution along the cup circumference at different heights, shown in Figure 3 (b), indicates that its trend is clearly underestimated. This is particularly evident for the top of the cup (height of 30 mm (H30)), for which the numerical simulation predicts a constant value, equal to the gap between the punch and the die (see Figure 1).

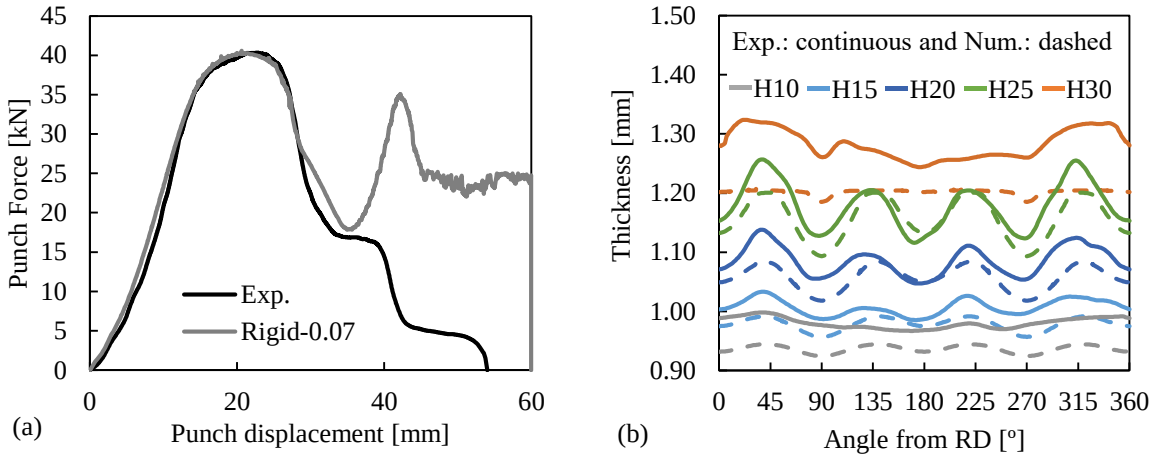

Figure 3. Comparison between experimental and predicted results using rigid tools, Hill'48 and μ=0.07: (a) punch force-displacement and (b) thickness distribution along the cup circumference at different heights H = 10, 15, 20, 25 and 30 mm from the cup bottom (Experimental: continuous line and Numerical: dashed line).

The thickness was experimentally measured using different techniques [3], all of which confirmed the occurrence of values higher than the gap between the punch and the die at the top of the cup. The tools were also measured using different techniques, which revealed deviations on dimensions related with the tools clearance in the order of ± 0.001 mm [3]. Therefore, unlike in [6], it is not possible to associate the thickness results with slight wear of the tools.

3. Finite Element Model: deformable tools

The forming tools were discretized with solid finite elements to allow considering their elastic deformation. As shown in Figure 1, the discretization adopted is quite coarse because a surface smoothing method is applied. The surface smoothing method is based on Nagata patches, following the procedure proposed in [7] for frictional contact problems between deformable bodies. This way, the discretization of the deformable tools in the curved surfaces is identical to the one used for the rigid tools, providing a similar shape error, resulting from the surface interpolation with Nagata patches.

The blank holder is controlled with an imposed displacement on its top face that increases linearly with the punch displacement, until a maximum value of 0.17 mm, when the blank loses contact with the blank holder. This allows to mimic the behaviour observed when using rigid tools. The blank discretization adopted is the same used in the simulation performed with rigid tools.

3.1. Tools stiffness

The mechanical behaviour of the forming tools is assumed elastic and isotropic (von Mises). Since the tools are made of steel, the elastic properties initially considered were a Young's modulus of 210 GPa (E=210) and a Poisson ratio of 0.30. Nevertheless, in order to evaluate the influence of the tools stiffness, a 3 time lower value was considered for the tools Young's modulus, i.e. a value of 70 GPa (E= 70) was also considered. The constant value for the friction coefficient was adjusted to fit the maximum experimental drawing force. In this case, a slightly smaller value of μ =0.06 was selected for both values of stiffness of the deformable tools.

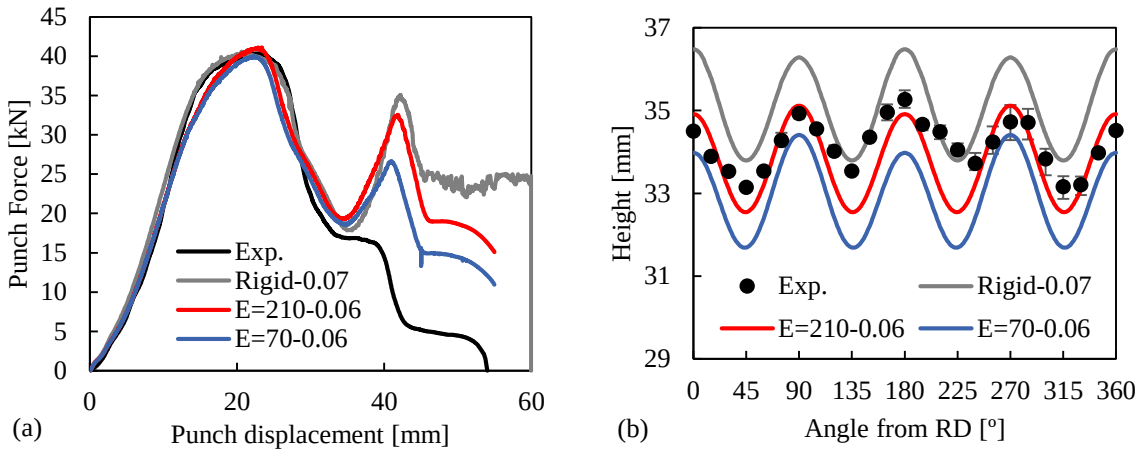

Figure 4. Comparison between experimental and predicted results using Hill'48 with rigid and deformable tools: (a) punch force-displacement and (b) earing profile.

Figure 4 (a) presents the comparison between the experimental and the numerical punch force evolution, confirming the small influence of the tools stiffness in the drawing stage. However, in the ironing stage, the punch force reduces with the decrease of the tools stiffness. The tools stiffness also has an impact on the cup height, as shown in Figure 4 (b). Note that the earing profile predicted with Hill'48 is similar to the experimental one, i.e. four ears with a minima at 45º. The average cup height decreases with the decrease of the tools stiffness. This is related with the fact that the magnitude of the friction force is proportional to the contact pressure. Thus, a lower tool stiffness generates lower friction

forces, contributing to a smaller cup with higher thickness values for the same height of the cup, as shown in Figure 5. The maximum values of thickness for each height are always predicted at 45º, which correlate with the minima height (see Figure 4 (b)). The increase of the tools stiffness leads to lower values of thickness, along the vertical wall of the cup and, consequently, to a higher average height. Note that the impact of the tools stiffness when considering deformable tools is mainly observed on the top of the vertical wall of the cup. Nevertheless, as shown in Figure 4 (a) the ironing force is still overestimated. Therefore, in the following section the influence of the friction coefficient is analysed.

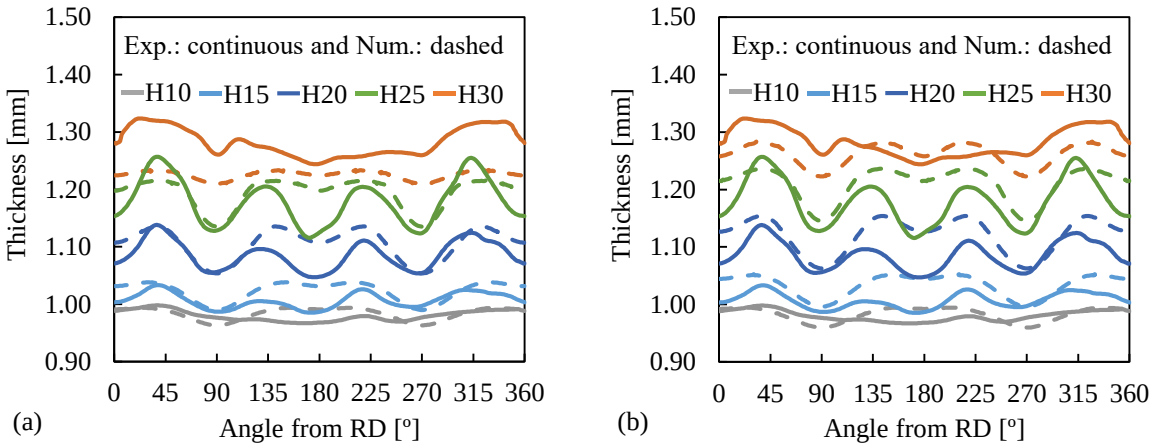

Figure 5. Comparison between experimental and predicted results using Hill'48 and deformable tools with μ=0.06, for the distribution of the thickness along the cup circumference at different heights (Experimental: continuous line and Numerical: dashed line): (a) E=210 GPa and (b) E=70 GPa.

3.2. Friction law

Numerical simulations were also performed with the deformable tools considering a null value for the friction coefficient, in order to evaluate the minimum value predicted for the punch force in the ironing stage. The analysis of the results, including the evolution of the contact pressure between the blank and the tools, enabled the definition of a pressure sensitive law for the friction coefficient. The friction law adopted is defined as follows:

$$\mu = B - (B - A)\exp\left(-mP^{n}\right) = 0.1\exp(-0.01P) \tag{5}$$

where P is the contact pressure (see e.g. [8]). When there is no contact $\mu = A = 0.1$ while for high contact pressure values μ will tend to the null value.

Figure 6 (a) shows that the evolutional friction law enables a more accurate global description of the punch force for both the drawing and the ironing stage, due to the reduction of the friction value with the increase of the contact pressure. It is also possible to observe that the ironing force is also sensitive to the tools stiffness, presenting lower values for the less stiff tools. The analysis of the cup height, presented in Figure 6 (b) indicates that this variable is more sensitive to changes in the friction coefficient value for the stiffer tools. It is also interesting to note that a similar earing profile is predicted for the stiffer tools, with a variable friction coefficient, and the softer tools, with the higher value for the friction coefficient. Nevertheless, in the last case the ironing force is clearly overestimated. Figure 7 presents the distribution of the thickness along the cup circumference at different heights, when considering the deformable tools with a null friction coefficient. The comparison with Figure 5 shows that the average thickness increases with the decrease of the friction coefficient. This is particularly evident for the intermediate heights of 15 and 20 mm, which justifies the lower average height (see Figure 6 (b)). Moreover, the change in thickness is not uniform along the cup circumferential coordinate.

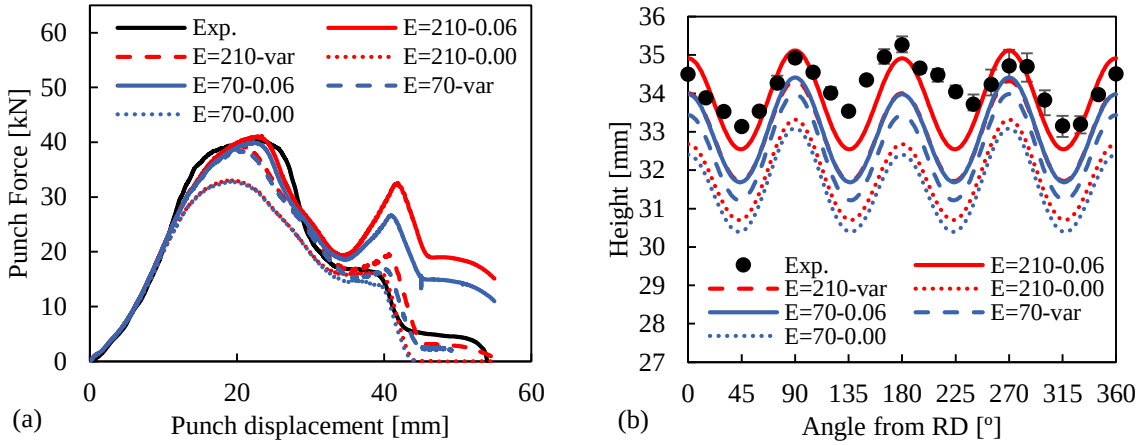

Figure 6. Comparison between experimental and predicted results using Hill'48, deformable tools and different values for the friction coefficient: (a) punch force-displacement and (b) earing profile.

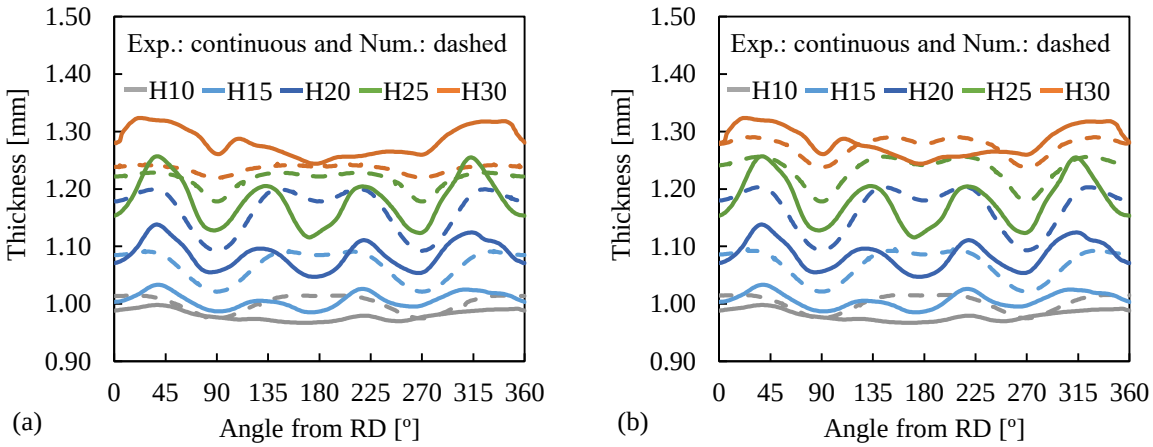

Figure 7. Comparison between experimental and predicted results using Hill'48, deformable tools and a null friction coefficient, for the evolution of the thickness along the cup circumference at different heights (Experimental: continuous line and Numerical: dashed line):
(a) E=210 GPa and (b) E=70 GPa.

Figure 8 (a) presents the contour plot of the norm of the radial nodal displacements in the less stiff tools, for a punch displacement of 40mm. Note that, according with the punch force evolution, this punch displacement corresponds to the ironing stage. Therefore, it is possible to see that the maximum deflection of the tools occurs in the plane (marked in red) corresponding to the transition between the die curvature radius and the vertical wall. The die presents a positive radial displacement while the punch presents a negative one, meaning that the gap between both tools increases. Figure 8 (b) compares the norm of the radial nodal displacements obtained in that plane, for both deformable tools and the two constant values of the friction coefficient. This confirms that the tools deflection decreases with the increase of the friction coefficient. Moreover, the tools deflection is higher between 0º and 45º to RD, i.e. where there is a greater thickening of the blank (see Figure 7), which is related with the lower *r*-value observed between 45º and 90º (see Figure 2 (a)). This also justifies the higher sensitivity of the thickness distribution along the circumferential direction to the friction value, for angles between 0º and 45º to RD.

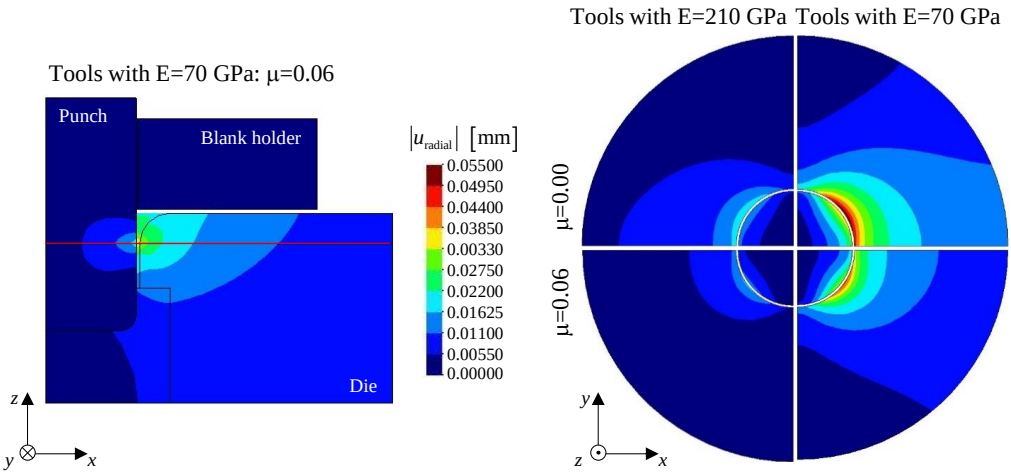

Figure 8. Contour plot of the norm of the radial nodal displacements [mm] in the tools for a punch displacement of 40 mm: (a) for the less stiff tools and (b) for both deformable tools and constant friction coefficient values, in the plane marked with the red line in (a).

Figure 9 presents the contour plot of the thickness strain, for a punch displacement of 35 mm, i.e. at the end of the drawing stage. Whatever the tools stiffness, for the higher friction coefficient value the thinning in the bottom of the cup is slightly higher while the thickening of the flange is slightly smaller. However, the thickness along the vertical wall of the cup is quite similar. This confirms the small impact of the tools stiffness in the drawing stage (see also Figure 4 (a)). The ironing of the vertical wall changes the thickness along the entire cup wall, even for relatively small ironing strains. The same was previously observed regarding the reduction in the residual stresses after ironing [9]. Although not shown here, the results obtained for the thickness distribution in the cup wall with the evolutional friction law are in between the ones reported for the two constant values of friction coefficient considered. This means that the average height of the cup is underestimated while the thickness values are overestimated, except for the highest height of 30 mm.

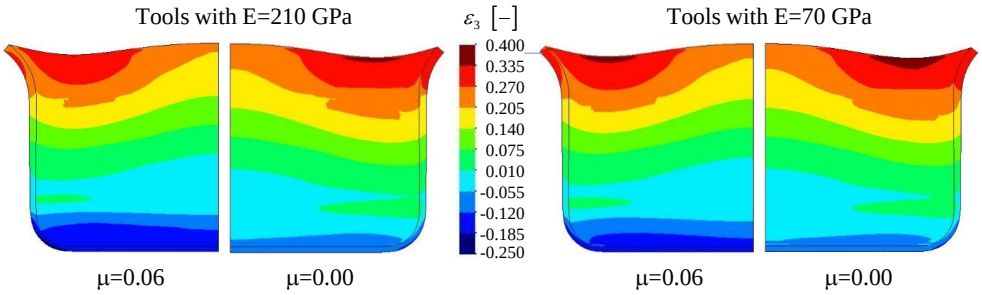

Figure 9. Contour plot of the thickness strain for a punch displacement of 35 mm.

3.3. Yield criteria

The thickness distribution is dictated by the normal to the yield surface since an associated flow rule is adopted. A numerical simulation was performed considering the stiffer deformable tools, the evolutional law for the friction coefficient and the CB2001 yield criterion. Figure 10 shows the evolution predicted for the punch force. The punch force predicted with the CB2001 is slightly lower than the one observed with the Hill'48, since the CB2001 predicts lower in-plane yield stress values (see Figure 2 (b)). In fact, the ironing force resembles more the one predicted with the less stiff tools. The same happens with the cup height at 0º, although at 90º the result is closer to the one obtained with the stiffer tools, as shown

in Figure 10 (b). This means that the CB2001 predicts an earing amplitude (3.86 mm) slightly higher than the Hill'48 (2.61 mm); both overestimate the experimental value (2.29 mm).

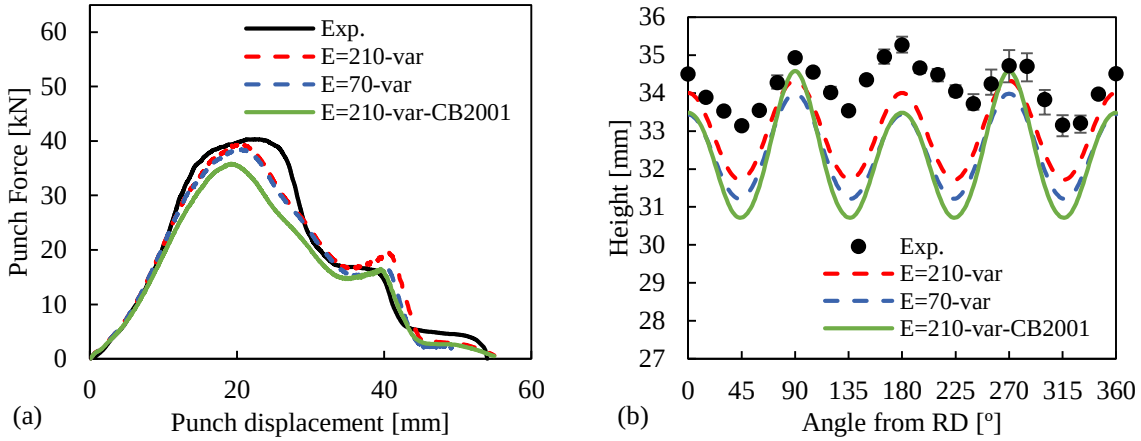

Figure 10. Comparison between experimental and predicted results considering deformable tools and an evolutional friction coefficient with the Hill'48 and the CB2001 yield criteria: (a) punch force-displacement and (b) earing profile.

Figure 11 (a) presents the distribution of the thickness along the cup circumference at different heights, predicted with the CB2001 yield criterion. The major differences with the values predicted with Hill'48 occur for angles between 45º and 90º. This results from the thickness distribution obtained at the end of the drawing stage, which presents lower thickening values for those directions, as shown in Figure 11 (b) (see also Figure 9). Note that the material initially located in the flange region is submitted to compression in the circumferential direction and tension in the radial one. Only for the material points in the free edge at RD and TD there will be a null component of the shear stress, meaning that the stress state is located in the compression-tension quadrant and the thickness strain is dictated by the normal to the yield surface in the region between uniaxial compression and pure shear stress states [10]. These corresponds to loading directions between 90º and 180º, which were not covered by the experimental tests performed, as shown in Figure 2 (d).

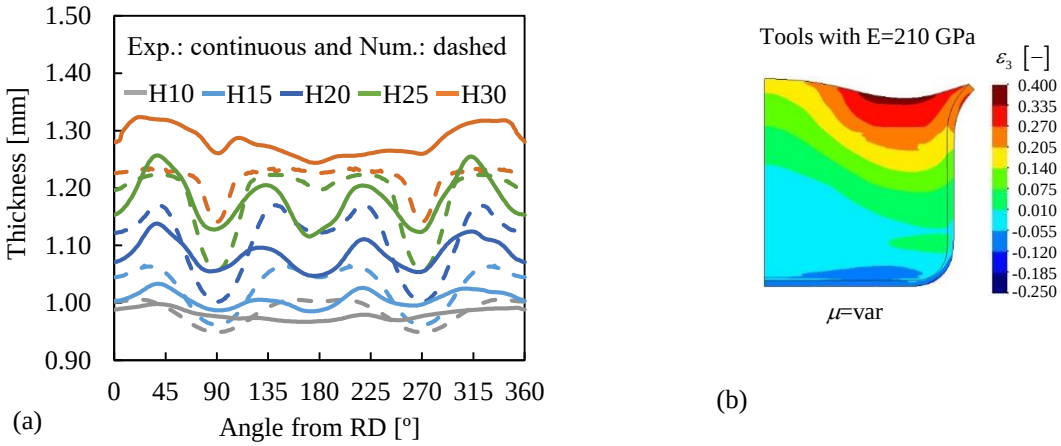

Figure 11. Comparison between experimental and predicted results considering deformable tools and an evolutional friction coefficient: (a) distribution of the thickness along the cup circumference at different heights with the Hill'48 and the CB2001 yield criteria (Experimental: continuous line and Numerical: dashed line) and (b) contour plot of the thickness strain for a punch displacement of 35 mm as predicted with the CB2001 yield criterion.

4. Conclusions

The analysis of the influence of the tools stiffness on the thickness distribution in a cylindrical cup wall was performed, showing that it affects not only the average value, at each height, but also the trend along the circumferential direction. This results from the orthotropic behaviour of the blank, which imposes a different thickening of the flange. Higher thickening values, associated with lower *r*-values, result in higher contact pressure values and, consequently, higher radial displacement of the tools. Nevertheless, the tool deflection is not enough to reduce the value of the punch force during the ironing stage. This force is quite sensitive to the friction coefficient, meaning that an evolutional friction law is required to enable capturing the drawing and ironing forces. The interaction between the tools stiffness and the friction law is highlighted by the similar earing profile predicted for the stiffer tools, with a variable friction coefficient, and the softer tools, with the higher value for the friction coefficient. This is related with similar thickness values excepted for the top of the cup. The thickness distribution at the end of the ironing stage is dictated by the one predicted at the end of the drawing stage, which requires improved knowledge about the direction of the plastic strain-rate in the compression-tension quadrant.

Acknowledgments

The authors gratefully acknowledge the financial support of the Portuguese Foundation for Science and Technology (FCT) under projects with reference PTDC/EME-EME/30592/2017 and PTDC/EME-EME/31657/2017 and by European Regional Development Fund (ERDF) through the Portugal 2020 program and the Centro 2020 Regional Operational Programme (CENTRO-01-0145-FEDER-031657) under the project UIDB/00285/2020.

References

[1] Neto D M, Coër J, Oliveira M C, Alves J L, Manach P Y and Menezes L F 2016 Numerical analysis on the elastic deformation of the tools in sheet metal forming processes *Int. J. Solids Struct.* **100** 270–85

[2] Vincze G and Habraken A 2021 EXACT - the ESAFORM Benchmark 2021 *ESAFORM 2021, 24th International Conference on Material Forming*

[3] Habraken A M, Toros A A, Alves J L, Amaral R L, Betaieb E, Chandola N, Corallo L, Cruz D J, Duchêne L, Engel B, Esener E, Firat M, Frohn-Sörensen P, Galán-López J, Ghiabakloo H, Kestens L, Lian J, Lingam R, Liu W, Ma J, Menezes L F, Nguyen-Minh T, Miranda S S, Neto D M, Pereira A F G, Prates P A, Reuter J, Revil-Baudard B, Rojas-Ulloa C, Sener B, Shen F, Van Bael A, Verleysen P, Barlat F, Cazacu O, Kuwabara T, Lopes A, Oliveira M C, Santos A D and Vincze G Analysis of ESAFORM 2021 cup drawing benchmark of an Al alloy , critical factors for accuracy and efficiency of FE simulations *Submitted to Int. J. Mater. Form.*

[4] Cazacu O and Barlat F 2001 Generalization of Drucker's yield criterion to orthotropy *Math. Mech. Solids* **6** 613–30

[5] Neto D M, Oliveira M C, Alves J L and Menezes L F 2015 Comparing faceted and smoothed tool surface descriptions in sheet metal forming simulation *Int. J. Mater. Form.* **8** 549–65

[6] Coër J, Laurent H, Oliveira M C, Manach P-Y and Menezes L F 2018 Detailed experimental and numerical analysis of a cylindrical cup deep drawing: Pros and cons of using solid-shell elements *Int. J. Mater. Form.* **11** 357–73

[7] Neto D M, Oliveira M C, Menezes L F and Alves J L 2016 A contact smoothing method for arbitrary surface meshes using Nagata patches *Comput. Methods Appl. Mech. Eng.* **299**

[8] Magny C 2002 Lois de frottement évolutives destinées à la simulation numérique de l'emboutissage *La Rev. Métallurgie* **99** 145–56

[9] Ragab M S and Orban H Z 2000 Effect of ironing on the residual stresses in deep drawn cups *J. Mater. Process. Technol.* **99** 54–61

[10] Oliveira M C, Cazacu O, Chandola N, Alves J L and Menezes L F 2021 On the effect of the ratio between the yield stresses in shear and in uniaxial tension on forming of isotropic materials *Mech. Res. Commun.* **114** 103693